2016 IEEE International Conference on Robotics and Automation (ICRA)
Stockholm, Sweden, May 16-21, 2016

A Comparison of the Yaw Constraining Performance of SCARA-Tau Parallel Manipulator Variants via Screw Theory

Mats Isaksson, Kristan Marlow, Torgny Brogårdh and Anders Eriksson

Abstract— **The SCARA-Tau parallel manipulator was derived with the objective to overcome the limited workspace-to-footprint ratio of the DELTA parallel manipulator while maintaining its many benefits. The SCARA-Tau family has later been extended and a large number of variants have been proposed. In this paper, we analyse four of these variants, which together encompass the main differences between all the proposed SCARA-Tau manipulators. The analysed manipulator variants utilise an identical arrangement of five of the six linkages connecting the actuated arms and the manipulated platform and exhibit the same input-output Jacobian. The normalised reciprocal product between the wrench of the sixth linkage and the twist of the platform occurring without this linkage provides a measure on how effectively the sixth linkage constrains the manipulated platform. A comparison of the manipulator variants with respect to this measure demonstrates each variants suitability for specific applications.**

I. Introduction

It is well known that parallel robots have the potential for improved accuracy and higher acceleration compared to similar-sized serial robots, while they typically suffer from a limited workspace-to-footprint ratio. The SCARA-Tau manipulator [1] was designed with the objective to extend the workspace-to-footprint ratio of the Delta mechanism designed by Clavel [2] while maintaining its many benefits. Several variants of the SCARA-Tau manipulator have later been proposed and partly analysed [3]–[6]. However, much of the previous analysis and comparison of the different variants have been focused on the input-output Jacobian, which does not consider the closeness to constraint singularities.

In this paper, we analyse the differences between four variants of the SCARA-Tau family. These variants were selected to encompass the main characteristics of the proposed SCARA-Tau variants while exhibiting the same input-output Jacobian. For the studied variants, five of the six distal linkages connecting the actuated rotating arms to the manipulated platform have an identical arrangement. Hence, analysing the motion/force transmission effectiveness of the sixth linkage is sufficient to compare these manipulators. The employed index is based on the power coefficient proposed by Wang et al. [7] and further discussed in [8]–[11], which measures the motion/force transmission effectiveness between a wrench and a twist.

The remainder of this paper is organised as follows. Section II introduces the SCARA-Tau family of parallel manipulators and provides previous results for these mechanisms. Section III defines the kinematic parameters of the investigated manipulator variants, while Section IV presents the index used to compare their performance. Section V provides a workspace analysis of the analysed variants, where each reachable position has been coloured according to the value of the employed performance index. Finally, Section VI provides conclusions and suggestions for future work.

II. The SCARA-Tau Family

The SCARA-Tau manipulator was invented and developed by ABB Robotics [1]. Fig. 1(a) shows the first full-scale prototype of this manipulator, while Fig. 1(b) provides a cutaway view of its CAD model. The analysed SCARA-Tau variants are three-degree-of-freedom (3-DOF) manipulators, composed of a central base column and an arm system that can rotate indefinitely around this column. All variants employ three actuated rotating proximal arms, where each arm is connected by 1–3 distal linkages to a manipulated platform. Each linkage is composed of a fixed-length link with a universal joint on the platform end and a spherical joint on the other end. As the links in such linkages are only susceptible to axial forces, they can be constructed from lightweight carbon fibre rods with the carbon filament mainly in the direction of the link. All actuators are mounted on the fixed base. As the entire arm system can rotate indefinitely around the central base column, the workspace does not suffer discontinuities requiring a large rotation of the arm

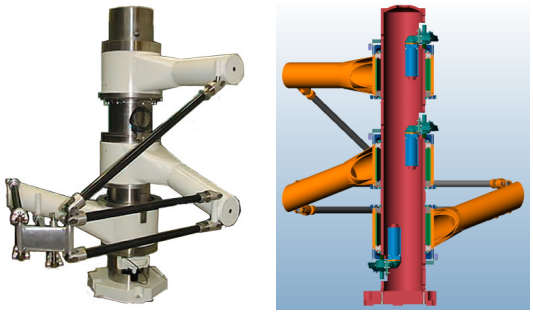

(a) Prototype (b) CAD model

Fig. 1. (a) The 2 m tall SCARA-Tau prototype. (b) A cutaway view of the CAD model of the prototype.

M. Isaksson is with the Electrical and Computer Engineering Department, Colorado State University, USA. E-mail: mats.isaksson@gmail.com. K. Marlow is with the Centre for Intelligent Systems Research (CISR), Deakin University, Australia. E-mail: kristan.marlow@research.deakin.edu.au. Torgny Brogårdh is an independent scholar based in Sweden, email:torgny.brogardh@gmail.com. A. Eriksson is with the School of Electrical Engineering and Computer Science, Queensland University of Technology, Australia. This research was in part supported by the Australian Research Council through the project DE130101775.

978-1-4673-8026-3/16/$31.00 ©2016 IEEE

system in order to move between neighbouring Cartesian positions. The workspace of the manipulator is toroidal-shaped. Due to its extensive workspace and its endless rotation, one manipulator can efficiently service multiple conveyor belts or multiple work stations surrounding the robot.

All SCARA-Tau variants include two parallelograms composed of the previously mentioned linkages arranged into two vertical planes; hereafter referred to as vertical parallelograms. Isaksson et al. [6] analysed a manipulated platform connected to a fixed base by two such parallelograms. It was proved that the system of constraint wrenches in such a mechanism loses rank if the two linkages in a parallelogram become collinear, which is not physically possible, or if the planes formed by the two parallelograms become parallel. Additionally, it was proved that if such constraint singularities are avoided, the reciprocal twist system does not include any roll or pitch of the manipulated platform.

For the original SCARA-Tau manipulator in Fig. 1(a), the distal linkages are grouped in clusters of three, two and one (3/2/1), where the linkages within each cluster are parallel. The kinematics and error parameters of this design have been analysed in [12], [13]. In addition to the previously mentioned constraint singularities, the original SCARA-Tau suffers from a constraint singularity if the horizontal projections of the linkages in the cluster of three become collinear. Due to this constraint singularity, configurations where the manipulated platform is very close to the base column or very far from the base column suffer from reduced stiffness [14].

All SCARA-Tau variants suffer from a coupled parasitic yaw rotation of the manipulated platform when the platform is moved radially or vertically. However, most potential industrial applications of a SCARA-Tau robot, such as pick-and-place, would require a fourth actuated joint to manipulate the yaw angle. As such a joint could compensate for the coupled yaw angle motion, the practical disadvantage of the parasitic motion is limited.

Brogårdh et al. [3] proposed a triangular SCARA-Tau variant, for which the projection of the cluster of three linkages in a horizontal plane form a triangle. This variant significantly reduces the parasitic yaw angle rotation of the manipulated platform [4]. An additional benefit is that this design eliminates the constraint singularities due to the horizontal parallelogram. Additional variants of the 3/2/1 clustering of the linkages were proposed by Isaksson et al. [5], where it was stated that a quadrilateral linkage arrangement minimises the parasitic yaw angle rotation of the manipulated platform. In such an arrangement, the cluster of three linkages form a shape between a parallelogram and a triangle when projected in a horizontal plane. In the same paper, SCARA-Tau variants with a 2/2/2 clustering of the linkages were introduced. Modifying the arrangement of the two linkages attached to the uppermost proximal arm leads to significantly different manipulator properties.

In this paper, we analyse the main differences between the 3/2/1 linkage clustering and the 2/2/2 linkage clustering, in addition to the properties of the described parallel and triangular linkage arrangements. These variants encompass the main differences between all proposed SCARA-Tau manipulators and differ mainly in how well the yaw angle rotation is constrained and how each arrangement affects the coupled parasitic platform rotation of the manipulated platform. In order to make the comparison of these properties distinct, we have selected to study the four manipulator variants illustrated in Fig. 2, for which five of the platform joints are collinear. These manipulators are identical except for the arrangement of one distal linkage. If the tool centre point (TCP) is on the axis defined by the five collinear joints, the four manipulators have identical input-output Jacobian.

The variants in Fig. 2(a) and (b) were included in the patent [1], while the variants in Fig. 2(c) and (d) were mentioned in [5].

III. Notation and Kinematics

Figure 3 shows the kinematic parameters and the coordinate systems required for the forthcoming analysis. The naming convention is exemplified for both a 3/2/1 configuration and a 2/2/2 configuration. The three actuated proximal arms are denoted by A_1-A_3, where arms closer to the base of the central column have lower indices. The two links forming the vertical parallelogram on A_1 are denoted by L_1 and L_2, while the two links forming the vertical parallelogram on A_2 are denoted by L_3 and L_4. The lowest link in each parallelogram is given the lowest index. The link attached to the lowest position on A_3 is denoted by L_5. In case of two links attached at the same height on A_3, L_5 is the link whose proximal arm joint has the shortest perpendicular distance

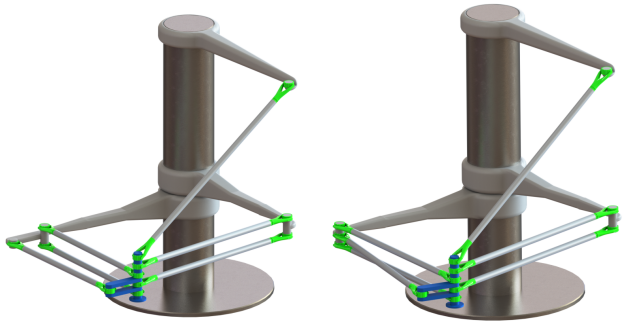

(a) Parallel 3/2/1 (b) Triangular 3/2/1

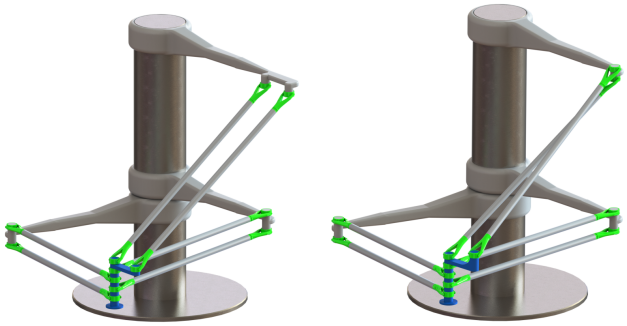

(c) Parallel 2/2/2 (d) Triangular 2/2/2

Fig. 2. The mechanisms in (a)-(d) have identical assembly of five of the six distal linkages.

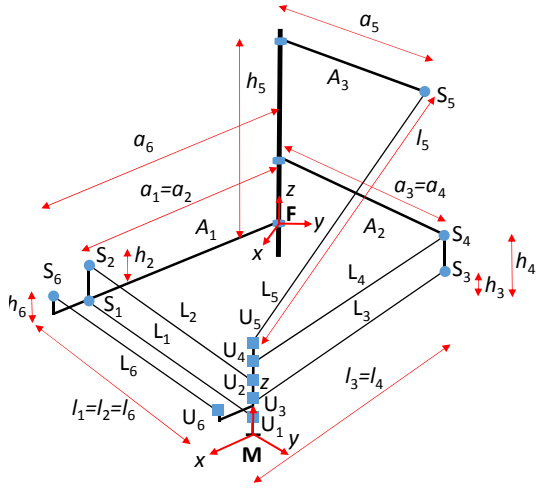

(a) 3/2/1 clustering

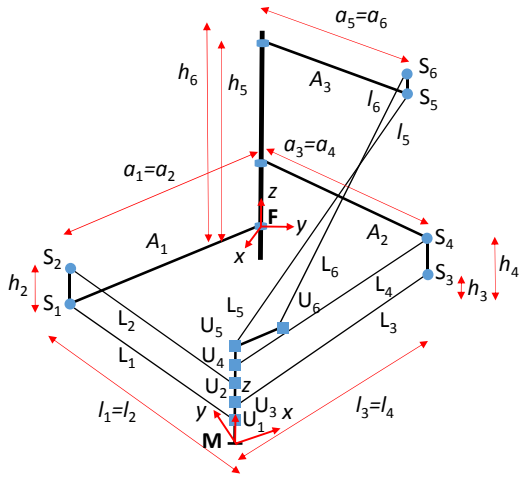

(b) 2/2/2 clustering

Fig. 3. Kinematic parameters. The employed naming convention is exemplified for one variant with a 3/2/1 clustering (a) and one variant with a 2/2/2 clustering (b).

to the central base column. The sixth link, mounted on A_1 for variants with a 3/2/1 clustering and on A_3 for variants with a 2/2/2 clustering, is denoted by L_6. Each link L_i is connected to a proximal arm by a spherical joint S_i and to the manipulated platform by a universal joint U_i. In order to simplify the kinematic descriptions, we will sometimes refer to the joint axes intersection point of S_i and U_i as the position or coordinate of these joints.

A coordinate system **F** is defined relative to the fixed base column. Its z-axis is defined by the common rotation axis of the three proximal arms and its xy-plane intersects joint S_1. Due to the axis-symmetry, the x-axis can be selected arbitrarily, while the y-axis is selected according to the right-hand rule.

The rotation angle of each proximal arm A_i is denoted by q_i, where the angles q_i are measured from the x-axis of **F**, with sign according to the right-hand rule.

The perpendicular distance between the joint axes intersection point of S_i and the rotation axis of the upper arms is denoted by a_i, while the kinematic length of each distal link L_i is denoted by l_i. The links in each parallelogram are of equal length ($l_1 = l_2$ and $l_3 = l_4$). The z-coordinate of each joint S_i in **F** is given by h_i, meaning h_1 is by definition equal to zero. Utilising these parameters, the coordinates of the spherical joints in **F** are given by

$$ {}^{\mathbf{F}}\mathbf{s}_1 = [a_1 \cos q_1, a_1 \sin q_1, h_1]^{\mathrm{T}} \tag{1} $$

$$ {}^{\mathbf{F}}\mathbf{s}_2 = [a_2 \cos q_1, a_2 \sin q_1, h_2]^{\mathrm{T}} \tag{2} $$

$$ {}^{\mathbf{F}}\mathbf{s}_3 = [a_3 \cos q_2, a_3 \sin q_2, h_3]^{\mathrm{T}} \tag{3} $$

$$ {}^{\mathbf{F}}\mathbf{s}_4 = [a_4 \cos q_2, a_4 \sin q_2, h_4]^{\mathrm{T}} \tag{4} $$

$$ {}^{\mathbf{F}}\mathbf{s}_5 = [a_5 \cos q_3, a_5 \sin q_3, h_5]^{\mathrm{T}} \tag{5} $$

$$ {}^{\mathbf{F}}\mathbf{s}_6 = \begin{cases} [a_6 \cos q_1, a_6 \sin q_1, h_6]^{\mathrm{T}}, & 3/2/1 \text{ clustering} \\ [a_6 \cos q_3, a_6 \sin q_3, h_6]^{\mathrm{T}}, & 2/2/2 \text{ clustering} \end{cases} \tag{6} $$

A coordinate system **M** is defined relative to the manipulated platform. As illustrated in Fig. 3, its z-axis is defined by the five collinear platform joints in the same direction as the z-axis of **F** and its origin is at the bottom of the tool platform. Its x-axis is defined by the perpendicular direction from the z-axis of **M** to the position of joint U_6 and the y-axis is selected according to the right-hand rule. We will refer to the origin of **M** as the TCP of the studied manipulators. The origin of **M** in **F** is given by the position vector $\mathbf{x} = [x, y, z]^{\mathrm{T}}$, while the rotation of **M** relative to **F** around the z-axis of **F** is defined by

$$ \mathbf{R} = \begin{bmatrix} \cos\phi & \sin\phi & 0 \\ -\sin\phi & \cos\phi & 0 \\ 0 & 0 & 1 \end{bmatrix}, \tag{7} $$

where ϕ is the platform yaw angle. The coordinates of the platform joints in **M** are given by

$$ \mathbf{u}_i = [u_{ix}, u_{iy}, u_{iz}]^{\mathrm{T}}. \tag{8} $$

For the calculation of the performance index, we also utilise the coordinates of the joints S_i expressed in **M**, which are given by

$$ \mathbf{s}_i = \mathbf{R}^{\mathrm{T}}({}^{\mathbf{F}}\mathbf{s}_i - \mathbf{x}) \tag{9} $$

For each investigated position **x**, the inverse kinematics presented in [15] is employed to find corresponding values of both the platform yaw angle ϕ and the joint angles q_i. Thereafter, the joint positions $\mathbf{u}_i$ and $\mathbf{s}_i$ are determined from (8) and (9), respectively.

IV. Performance Index

The performance of a manipulator is affected at singular locations as well as in configurations close to a singularity. Therefore, an index that measures the closeness between a pose and a singular configuration is beneficial. In this paper, we employ the power coefficient proposed by Wang et al. [7], which in turn is an adaption of the work by Sutherland and Roth [16]. Implementations of the power coefficient are exemplified in [8]–[11]. The power coefficient represents the motion/force transmission effectiveness between a wrench

and a twist. It can be applied to purely translational, purely rotational and combined motion parallel manipulators [9]. The power coefficient is defined as

$$\rho = \frac{\left|\hat{\$}_1 \circ \hat{\$}_2\right|}{\left|\hat{\$}_1 \circ \hat{\$}_2\right|_{\max}}, \tag{10}$$

where the numerator is the reciprocal product between a unit wrench $\hat{\$}_1$ and unit twist $\hat{\$}_2$, and the denominator is the maximum magnitude of this reciprocal product, as succinctly defined in [8].

A mechanism's constraint performance is associated with its output transmission ability [8], and therefore, an analysis of its output motion/force transmission effectiveness is performed. A mechanism's output transmission ability is calculated through application of the power coefficient (10) on its wrenches and their respective output twists. The corresponding output twist for a wrench is defined as the free motion of the mobile platform if the wrench under examination is suppressed. It represents the reciprocal twist that describes the mobile platform's free motion [17].

All the manipulator variants examined in this paper include closed-loop sub-chains (CLSCs), as seen in the distal link grouping of chains one and two in Fig. 3(a) and chains one, two and three in Fig. 3(b). Screw theory based singularity analysis of such mechanisms is commonly performed by reducing the CLSCs into their equivalent constraint and actuation wrenches [18], [19]. However, as discussed in [14], when performing motion/force transmission analysis of mechanisms with CLSCs, such simplifications result in important information about the constraint produced by a CLSC itself being lost. Therefore, in the following analysis, we utilise the unreduced wrenches directed along each of the distal links.

Herein, we are only concerned with each mechanism's ability to constrain the mobile platform's yaw rotation. This rotation is directly constrained by link L_6. Therefore, the wrench of interest is the zero pitch wrench passing through joints S_6 and U_6, as seen in Fig. 4. It is defined by

$$\hat{\$}_{C6} = \begin{bmatrix} \mathbf{d}_6 \\ \mathbf{u}_6 \times \mathbf{d}_6 \end{bmatrix}, \tag{11}$$

where

$$\mathbf{d}_6 = \frac{\mathbf{u}_6 - \mathbf{s}_6}{|\mathbf{u}_6 - \mathbf{s}_6|} \tag{12}$$

is the unit vector between joint S_6 and U_6, calculated using (8) and (9).

For each of the mechanisms in Fig. 2, the output twist gained when the wrench $\hat{\$}_{C6}$ of the yaw constraining link L_6 is suppressed, is a zero pitch twist along the five collinear platform joints. It is given by

$$\hat{\$}_{O6} = \begin{bmatrix} \hat{\mathbf{z}} \\ \mathbf{0}_{3\times 1} \end{bmatrix}, \tag{13}$$

where $\hat{\mathbf{z}}$ is a unit vector parallel to the z-axis of $\mathbf{M}$ in Fig. 3. If $\hat{\$}_{C6}$ becomes reciprocal to $\hat{\$}_{O6}$, that is, if

$$\hat{\$}_{C6} \circ \hat{\$}_{O6} = 0, \tag{14}$$

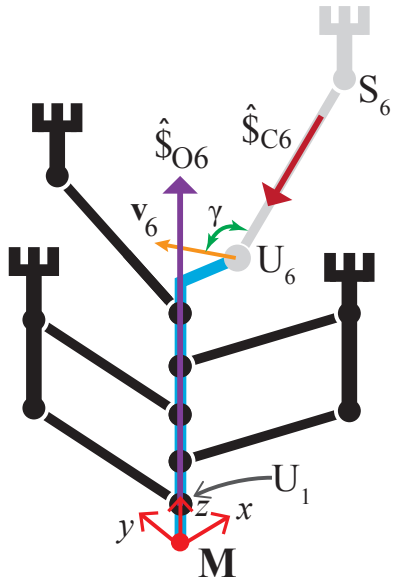

Fig. 4. Wrench and output twist associated with the calculation of ρ_6. This illustration is for the general case and applicable to all the investigated variants.

the mechanism's yaw constraint is lost.

The yaw constraints performance is calculated by applying the power coefficient to (11) and (13),

$$\begin{aligned}\rho_6 &= \frac{\left|\hat{\$}_{C6} \circ \hat{\$}_{O6}\right|}{\left|\hat{\$}_{C6} \circ \hat{\$}_{O6}\right|_{\max}} = \frac{|(\mathbf{u}_6 \times \mathbf{d}_6) \cdot \hat{\mathbf{z}}|}{|(\mathbf{u}_6 \times \mathbf{d}_6) \cdot \hat{\mathbf{z}}|_{\max}} \\ &= \frac{|\mathbf{d}_6 \cdot (\hat{\mathbf{z}} \times \mathbf{u}_6)|}{|\mathbf{d}_6 \cdot (\hat{\mathbf{z}} \times \mathbf{u}_6)|_{\max}} = \frac{|\mathbf{d}_6 \cdot \mathbf{v}_6|}{|\mathbf{d}_6 \cdot \mathbf{v}_6|_{\max}},\end{aligned} \tag{15}$$

where

$$\mathbf{v}_6 = \hat{\mathbf{z}} \times \mathbf{u}_6 = \begin{bmatrix} 0 \\ 0 \\ 1 \end{bmatrix} \times \begin{bmatrix} u_{6x} \\ 0 \\ u_{6z} \end{bmatrix} = \begin{bmatrix} 0 \\ u_{6x} \\ 0 \end{bmatrix} \tag{16}$$

is the velocity vector of the joint axes intersection point of the universal joint U_6. The expression (15) can be further simplified to

$$\rho_6 = \frac{|\mathbf{d}_6 \cdot \mathbf{v}_6|}{|\mathbf{d}_6 \cdot \mathbf{v}_6|_{\max}} = \frac{|\mathbf{d}_6|\,|\mathbf{v}_6|\,|\cos\gamma|}{|\mathbf{d}_6|\,|\mathbf{v}_6|} = |\cos\gamma|, \tag{17}$$

where γ is the spatial angle between the velocity vector $\mathbf{v}_6$ and the screw axis of $\hat{\$}_{C6}$, illustrated in Fig. 4.

As evident from (17), the index is finite, dimensionless and frame invariant, with a range from zero to unity. Unity represents the furthest locations from a singularity and zero occurs at singular locations. Hence, the index ρ_6 provides a measure of the effectiveness of the yaw constraining linkage.

V. Constrainability Analysis

In this section, the index ρ_6 (17) is utilised to compare the yaw constraining performance of the manipulators in Fig. 2. To visualise the performance distribution throughout the manipulators' workspace, a two dimensional quasi-random set of 10^6 points was generated with bounds of $0 \le x \le (a_1 + l_1)$ and $-l_1 - u_{1z} \le z \le l_1 - u_{1z}$. The kinematic parameters of

the four analysed manipulator variants are listed in Table I. For the studied manipulators, all parameters except those determining the arrangement of the yaw constraining link L_6 are identical. Due to collisions between the distal linkages and the base column, a thin section of the workspace close to the base column is not reachable. As the size of this section depends on the radii of the base column and the distal linkages, this limitation has not been included in the workspace plots. Friction and gravity are not considered in this analysis.

The distribution plots of ρ_6 for the four variants are presented in Fig. 5. The plots show cross-sections of the toroidal-shaped workspace of each studied manipulator variant. Each plot is coloured according to the colour bar shown in Fig. 5(e), with low constraint performance coloured blue through to optimal constraint performance as red. The distribution plots enable intuitive interpretation and immediate visual comparison of the constraint performance of each manipulator variant. As two coplanar zero pitch screws are reciprocal, regions with low constraint performance correspond to configurations where the wrench $\hat{\$}_{C6}$ and the twist $\hat{\$}_{O6}$ are either close to intersecting or close to parallel.

Figure 5(a) shows the ρ_6 distribution for the SCARA-Tau variant with a 3/2/1 linkage clustering, in which L_6 is parallel to L_1 and L_2, as illustrated in Fig. 2(a). It is evident from the plot that this arrangement of L_6 results in an optimal yaw constraint towards the lower front of the workspace. The workspace sections with higher value of ρ_6 may be shifted along the x-axis by modifying the horizontal position of joint S_6 while maintaining its distance to S_1.

Figure 5(b) illustrates the distribution plot of ρ_6 for the SCARA-Tau variant with a 3/2/1 linkage clustering, in which the horizontal projections of L_1 and L_6 form a triangle, as illustrated in Fig. 2(b). It can be seen that this variant constrains the platform's yaw well in all locations, excluding the uppermost regions of the workspace. As evident, the triangular arrangement leads to a constant yaw constraint efficiency during radial motions of the manipulated platform. The reason is that the triangular shape formed by the horizontal projections of L_1 and L_6 remains constant during such a motion.

Figure 5(c) shows the distribution plot of ρ_6 for the SCARA-Tau variant with a 2/2/2 linkage clustering, in which

TABLE I

KINEMATIC PARAMETERS FOR THE MANIPULATORS IN FIG. 2. THE PARAMETERS FOR i=1–5 ARE IDENTICAL FOR ALL FOUR VARIANTS. THE UNIT OF ALL PARAMETERS IS METERS.

i	a_i	l_i	h_i	u_{ix}	u_{iy}	u_{iz}
1	0.900	1.100	0.000	0.000	0.000	0.055
2	0.900	1.100	0.110	0.000	0.000	0.165
3	0.900	1.100	0.055	0.000	0.000	0.110
4	0.900	1.100	0.165	0.000	0.000	0.220
5	0.900	1.300	1.000	0.000	0.000	0.275
6 (Fig. 2(a))	1.100	1.100	0.055	0.200	0.000	0.110
6 (Fig. 2(b))	0.900	1.100	0.055	0.200	0.000	0.110
6 (Fig. 2(c))	1.100	1.300	1.000	0.200	0.000	0.275
6 (Fig. 2(d))	0.900	1.300	1.055	0.200	0.000	0.330

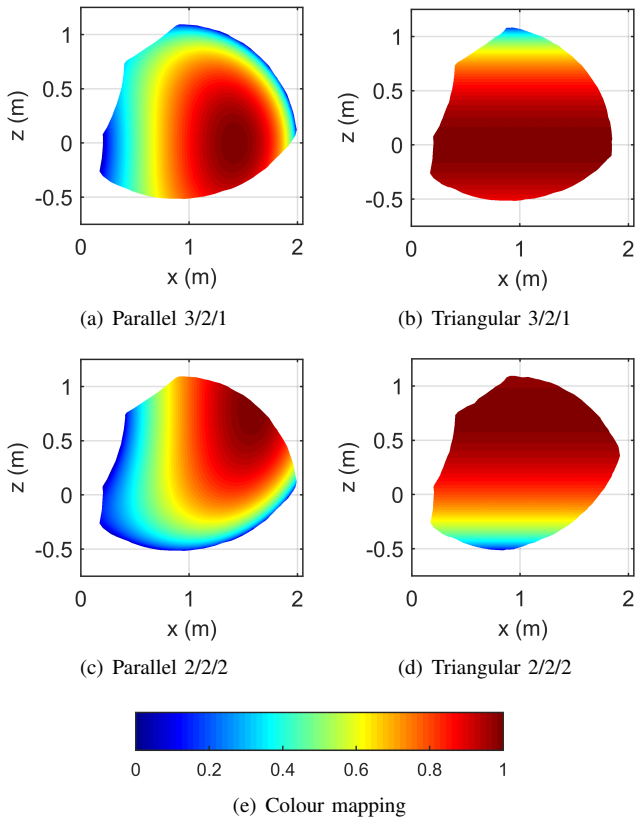

Fig. 5. The plots (a)–(d) illustrate cross-sections ($x \geq 0,\ y = 0$) of the toroidal-shaped workspace of the manipulators in Fig. 2. Due to the axis symmetry, the workspace and workspace properties are identical in all other radial half planes. Each analysed manipulator position is coloured depending on the value of ρ_6, according to the colour bar in (e).

L_6 is parallel to L_5, as shown in Fig. 2(c). Mounting link L_6 on the uppermost proximal arm shifts the optimally constrained region to the upper front of the workspace, resulting in poor constraint performance in the lower workspace. Similar to the variant in Fig. 2(a), the workspace sections with higher ρ_6 may be shifted along the x-axis by modifying the horizontal position of joint S_6 while maintaining its distance to S_5.

Figure 5(d) shows the distribution plot of ρ_6 for the SCARA-Tau variant with a 2/2/2 linkage clustering, in which the horizontal projections of L_5 and L_6 form a triangle, as illustrated in Fig. 2(d). As can be seen, this variant generally displays a high value of ρ_6; however, with reduced performance in the lower sections of the workspace. The ρ_6 distribution in Fig. 5(d) is essentially inverted when compared to the plot in Fig. 5(b). For applications such as pick-and-place, where the lower section of the workspace is the most important, a 3/2/1 linkage configuration is clearly preferable. However, for other applications, such as performing a task on the inside of a cylindrical body, the 2/2/2 configuration is a viable alternative.

The different arrangements of the yaw constraining linkage induce varying degrees of unwanted coupled parasitic yaw rotation during radial and vertical platform motions. Fig. 6 shows cross-sections of the toroidal-shaped workspace of

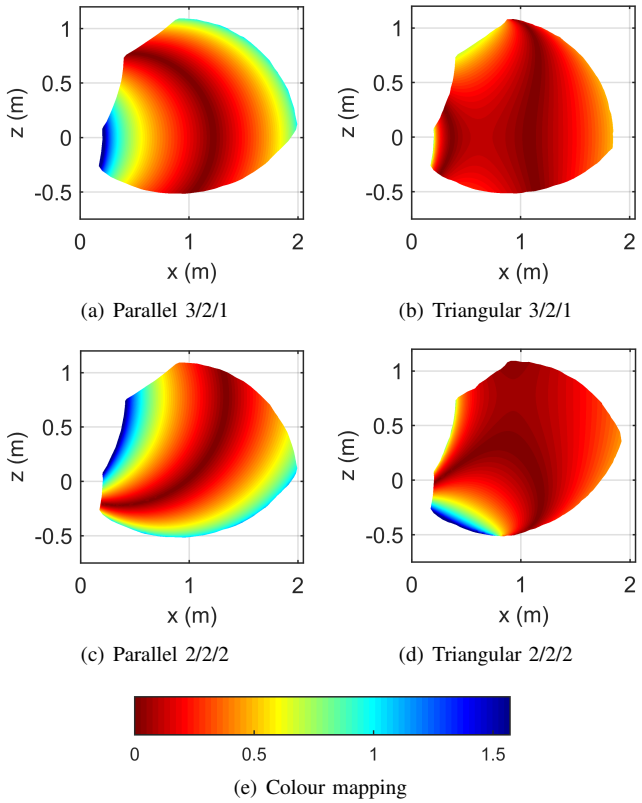

(a) Parallel 3/2/1 (b) Triangular 3/2/1

(c) Parallel 2/2/2 (d) Triangular 2/2/2

(e) Colour mapping

Fig. 6. The plots (a)–(d) illustrate cross-sections $(x \geq 0,\ y = 0)$ of the toroidal-shaped workspace of the manipulators in Fig. 2. Due to the axis symmetry, the workspace and workspace properties are identical in all other radial half planes. Each analysed manipulator position is coloured depending on the value of the absolute deviation of the yaw angle ϕ from its mean value, according to the colour bar in (e). The angular deviation is calculated in radians.

the studied manipulator variants. Each position is coloured according to the absolute deviation of the yaw angle ϕ in (7) from its mean value according to the color map in Fig. 6(e). The mean value of ϕ is different for each manipulator variant; however, this value does not affect the performance of the manipulators and can be compensated for by a fixed platform offset. Note that the colour map in Fig. 6(e) is inverted compared to the one in Fig. 5(e), meaning that values in red indicate an advantageous performance of the manipulator for all plots in this paper. As can be seen by comparing the plots in Fig. 6, the triangular arrangements lead to a substantial reduction of the coupled parasitic yaw angle rotation.

VI. Conclusion and Future Work

In this paper, we employed the power coefficient to analyse the yaw constraining performance of different members of the SCARA-Tau family of parallel manipulators. By selecting the kinematic parameters of the analysed variants to be identical, except for those controlling the analysed property, we achieved a distinct comparison between the main SCARA-Tau variants. The results provide a strong indication of the benefits of a triangular linkage arrangement and shows that for applications mainly utilising the lower section of the workspace, such as pick-and-place, a 3/2/1 linkage clustering is preferable.

Suggested future work includes extending the presented analysis to all six distal linkages of a SCARA-Tau manipulator. That is, evaluating the power coefficient of the wrench generated by each linkage and its respective output twist, thereby completely characterising the motion/force transmission capability of these mechanisms.

References

[1] S. Kock, R. Oesterlein, and T. Brogårdh, "Industrial robot," WO Patent 03/066289 A1, Aug. 14, 2003.

[2] R. Clavel, "Device for the movement and positioning of an object in space," US Patent 4,976,582, Dec. 11, 1990.

[3] T. Brogårdh, S. Hanssen, and G. Hovland, "Application-Oriented Development of Parallel Kinematic Manipulators with Large Workspace," in *2nd International Colloquium of the Collaborative Research Center, 562: Robotic Systems for Handling and Assembly*, Braunschweig, Germany, 2005, pp. 153–170.

[4] M. Isaksson, T. Brogårdh, I. Lundberg, and S. Nahavandi, "Improving the Kinematic Performance of the SCARA-Tau PKM," in *IEEE International Conference on Robotics and Automation (ICRA'10)*, Anchorage, AK, USA, 2010, pp. 4683–4690.

[5] M. Isaksson, T. Brogårdh, and S. Nahavandi, "Parallel Manipulators with a Rotation-Symmetric Arm System," *Journal of Mechanical Design*, vol. 134, no. 11, 114503, 2012.

[6] M. Isaksson, A. Eriksson, M. Watson, T. Brogårdh, and S. Nahavandi, "A method for extending planar axis-symmetric parallel manipulators to spatial mechanisms," *Mechanism and Machine Theory*, vol. 83, pp. 1–13, 2015.

[7] J. Wang, C. Wu, and X.-J. Liu, "Performance evaluation of parallel manipulators: Motion/force transmissibility and its index," *Mechanism and Machine Theory*, vol. 45, no. 10, pp. 1462–1476, 2010.

[8] X.-J. Liu, C. Wu, and J. Wang, "A New Approach for Singularity Analysis and Closeness Measurement to Singularities of Parallel Manipulators," *Journal of Mechanisms and Robotics*, vol. 4, no. 4, 041001, 2012.

[9] F. Xie, X.-J. Liu, and J. Li, "Performance Indices for Parallel Robots Considering Motion/Force Transmissibility," in *Intelligent Robotics and Applications*. Springer, 2014, pp. 35–43.

[10] X.-J. Liu, X. Chen, and M. Nahon, "Motion/Force Constrainability Analysis of Lower-Mobility Parallel Manipulators," *Journal of Mechanisms and Robotics*, vol. 6, no. 3, 031006, 2014.

[11] H. Liu, M. Wang, T. Huang, D. G. Chetwynd, and A. Kecskeméthy, "A Dual Space Approach for Force/Motion Transmissibility Analysis of Lower Mobility Parallel Manipulators," *Journal of Mechanisms and Robotics*, vol. 7, no. 3, 034504, 2015.

[12] Z. Zhu, J. Li, Z. Gan, and H. Zhang, "Kinematic and dynamic modelling for real-time control of Tau parallel robot," *Mechanism and Machine Theory*, vol. 40, no. 9, pp. 1051–1067, 2005.

[13] H. Cui, Z. Zhu, Z. Gan, and T. Brogårdh, "Kinematic analysis and error modeling of TAU parallel robot," *Robotics and Computer Integrated Manufacturing*, vol. 21, no. 6, pp. 497–505, 2005.

[14] K. Marlow, M. Isaksson, J. S. Dai, and S. Nahavandi, "Motion/Force Transmission Analysis of Parallel Mechanisms with Planar Closed-Loop Sub-Chains," *Journal of Mechanical Design*, In press.

[15] M. Isaksson, A. Eriksson, and S. Nahavandi, "Analysis of the Inverse Kinematics Problem for 3-DOF Axis-Symmetric Parallel Manipulators with Parasitic Motion," in *IEEE International Conference on Robotics and Automation (ICRA'14)*, Hong Kong, China, 2014, pp. 5736–5743.

[16] G. Sutherland and B. Roth, "A Transmission Index for Spatial Mechanisms," *Journal of Engineering for Industry*, vol. 95, no. 2, pp. 589–597, 1973.

[17] J. S. Dai and J. R. Jones, "Interrelationship between screw systems and corresponding reciprocal systems and applications," *Mechanism and Machine Theory*, vol. 36, no. 5, pp. 633–651, 2001.

[18] S. Amine, D. Kanaan, S. Caro, and P. Wenger, "Constraint and Singularity Analysis of Lower-Mobility Parallel Manipulators with Parallelogram Joints," in *ASME 2010 IDETC/CIE*. American Society of Mechanical Engineers, 2010, pp. 1317–1326.

[19] H. Fang, Y. Fang, and K. Zhang, "Reciprocal screw theory based singularity analysis of a novel 3-dof parallel manipulator," *Chinese Journal of Mechanical Engineering*, vol. 25, no. 4, pp. 647–653, 2012.